doi:10.1016/j.jmb.2011.03.046 J. Mol. Biol. (2011) 408, 815–824

Contents lists available at www.sciencedirect.com

Journal of Molecular Biology

journal homepage: http://ees.elsevier.com.jmb

COMMUNICATION

Two Modes of Binding of DinI to RecA Filament Provide a New Insight into the Regulation of SOS Response by DinI Protein

Vitold E. Galkin[1]*, Rachel L. Britt[2], Lukas B. Bane[2], Xiong Yu[1], Michael M. Cox[2] and Edward H. Egelman[1]

[1]*Department of Biochemistry and Molecular Genetics, University of Virginia, Jordan Hall 6007, 1340 Jefferson Park Avenue, Charlottesville, VA 22908, USA*
[2]*Department of Biochemistry, University of Wisconsin-Madison, 433 Babcock Drive, Madison, WI 53706-1544, USA*

Received 1 February 2011; received in revised form 20 March 2011; accepted 22 March 2011
Available online 31 March 2011

Edited by J. Karn

Keywords:
RecA filament;
DinI;
bacterial SOS response;
LexA cleavage;
homologous recombination

RecA protein plays a principal role in bacterial SOS response to DNA damage. The induction of the SOS response is well understood and involves the cleavage of the LexA repressor catalyzed by the RecA nucleoprotein filament. In contrast, our understanding of the regulation and termination of the SOS response is much more limited. RecX and DinI are two major regulators of RecA's ability to promote LexA cleavage and strand exchange reaction, and are believed to modulate its activity in ongoing SOS events. DinI's function in the SOS response remains controversial, since its interaction with the RecA filament is concentration dependent and may result in either stabilization or depolymerization of the filament. The 17 C-terminal residues of RecA modulate the interaction between DinI and RecA. We demonstrate that DinI binds to the active RecA filament in two distinct structural modes. In the first mode, DinI binds to the C-terminus of a RecA protomer. In the second mode, DinI resides deeply in the groove of the RecA filament, with its negatively charged C-terminal helix proximal to the L2 loop of RecA. The deletion of the 17 C-terminal residues of RecA favors the second mode of binding. We suggest that the negatively charged C-terminus of RecA prevents DinI from entering the groove and protects the RecA filament from depolymerization. Polymorphic binding of DinI to RecA filaments implies an even more complex role of DinI in the bacterial SOS response.

Published by Elsevier Ltd.

Introduction

RecA is a key player in maintaining the integrity of the bacterial genome. It is crucial for DNA repair via homologous recombination and is required for the induction of SOS response in bacteria.[1–3] The RecA protein of *Escherichia coli* contains 352 amino acid residues and consists of a large core domain and a smaller C-terminal domain (CTD; residues 271–352). The last 24 residues were found to be disordered in all crystal structures,[4–8] except in *Mycobacterium*

*Corresponding author. E-mail address: galkin@virginia.edu.

Abbreviations used: CTD, C-terminal domain; dsDNA, double-stranded DNA; ssDNA, single-stranded DNA; 3D, three-dimensional; PDB, Protein Data Bank; IHRSR, Iterative Helical Real-Space Reconstruction.

0022-2836/$ - see front matter. Published by Elsevier Ltd.

smegmatis RecA complexed with dATP.[9] Most bacterial RecA proteins contain a high concentration of negatively charged residues at their C-terminus.[10]

Double-stranded DNA (dsDNA) breakages or stalled replication forks produce regions of single-stranded DNA (ssDNA). Polymerization of RecA monomers on ssDNA initiates the transcription of more than 40 proteins involved in the SOS response in bacteria.[11] Synthesis of these proteins is normally inhibited by the LexA repressor, which can cleave itself[12] upon binding within the helical groove of the RecA–DNA filament.[13] Also, the RecA–DNA filament acts as an ATP-dependent recombinase and is capable of promoting DNA pairing and strand exchange.[14] The repair of the damaged dsDNA results in degradation of ssDNA and depolymerization of the RecA nucleoprotein filaments, which in turn restores the pool of LexA repressor and shuts down the SOS system.

To prevent undesired DNA rearrangements, bacteria developed a sophisticated system to control the formation of the RecA–ssDNA filament. RecA activity is modulated by its C-terminus in a Mg^{2+}-dependent fashion.[15] Deletion of the 25 C-terminal residues results in faster RecA nucleation.[16] The 17 C-terminal RecA residues prevent binding of RecA to dsDNA (favoring RecA polymerization on ssDNA) and modulate RecA's ability to displace SSB protein from ssDNA.[17] Recently, crystal structures of the RecA–ssDNA/dsDNA filaments have been solved,[18] but these did not provide any structural information about the RecA C-terminus because this region was used as a linker to construct a RecA polypeptide.

The two other well-known modulators of RecA filaments are RecX and DinI. RecX protein is an intrinsic inhibitor of RecA activities, and overexpression of RecA in the absence of the *recX* gene is toxic to bacteria.[19,20] RecX inhibits the RecA-dependent strand exchange reaction and coprotease activity by slow depolymerization of RecA–DNA filaments.[21,22] Similarly to LexA, RecX binds deep in the helical groove of RecA filaments.[13] The competition between LexA and RecX for binding within the RecA helical groove may contribute to the inhibition of LexA cleavage by RecX. Removal of the 17 C-terminal RecA residues (RecAΔC17) significantly alters the ability of RecX to inhibit the strand exchange reaction and DNA-dependent ATPase activity.[23]

Another member of the SOS regulon is the *dinI* gene, which encodes a small protein containing 81 amino acid residues.[24,25] Originally, it was shown that the overexpression of DinI protein conferred severe UV sensitivity on wild-type cells and resulted in the inhibition of LexA and UmuD cleavage.[26] Later, it was suggested that, under normal expression levels, DinI would inhibit UmuD cleavage to limit SOS mutagenesis while having little effect on LexA processing.[26] The role of DinI as a down-regulator of the SOS response was also supported by the observation that the maximum binding of DinI to RecA filaments occurred at later stages of the SOS response.[27] It was proposed that a negatively charged C-terminal helix in DinI could compete with ssDNA for binding to the L2 loop of RecA, which in turn would displace ssDNA from the RecA nucleoprotein filament and inhibit the strand exchange reaction.[27] At a stoichiometric ratio of DinI to RecA, DinI displays a substantial stabilizing effect on the RecA filament.[28] It also allows LexA cleavage and does not interfere with an ongoing strand exchange reaction. The deletion of the 17 C-terminal residues of RecA has a dramatic effect on RecA–DinI interaction[28]—it alters DinI affinity for the RecA filament. In contrast to the wild-type RecA, RecAΔC17 has reduced strand exchange activity when DinI is present. We used electron microscopy and image analysis to locate the binding site of DinI on the RecA filament and to explore the structural consequences of the deletion of the 17 C-terminal residues of RecA on its ability to interact with DinI.

Results and Discussion

The formation of the RecA filament requires ATP binding, but ATP hydrolysis is not required for coprotease activity[29] or for the catalysis of the strand exchange reaction.[30] In the presence of ATP, RecA forms disordered filaments due to protomer dissociation upon ATP hydrolysis. Such filaments are inappropriate for image analysis. We have shown previously that the long and ordered RecA filaments formed in the presence of nonhydrolyzable ATP analogs are in an active extended conformation.[31] In this study, we used AMP-PNP to form RecA–DNA or RecAΔC17–DNA filaments alone (Fig. 1a and b), or in the presence of DinI (Fig. 1c and d). We extracted 6381 segments of RecA and 5198 segments of RecAΔC17 to generate three-dimensional (3D) reconstructions of those filaments (Fig. 2a). Both sets converged to a pitch of ~92 Å, consistent with the extended "active" form of the filament. Paradoxically, wild-type RecA reconstruction possessed a weaker electron density in the CTD region than the RecAΔC17 reconstruction (Fig. 2a, red arrowheads); otherwise, the two reconstructions were similar. This was consistent with our previous observations that the deletion of 18 C-terminal residues resulted in conformational changes in the CTD.[32] Recently, crystal structures of RecA–ssDNA/dsDNA filaments have been solved.[18] Since our filaments were formed on dsDNA, we used the high-resolution structure of the RecA–dsDNA filament [Protein Data Bank (PDB) ID: 3CMT] to evaluate the reconstruction of the RecAΔC17 filament. At a resolution of ~23 Å, no perturbations of the original crystal structure were required to dock it into the electron density map (Fig. 2b). This suggests that no

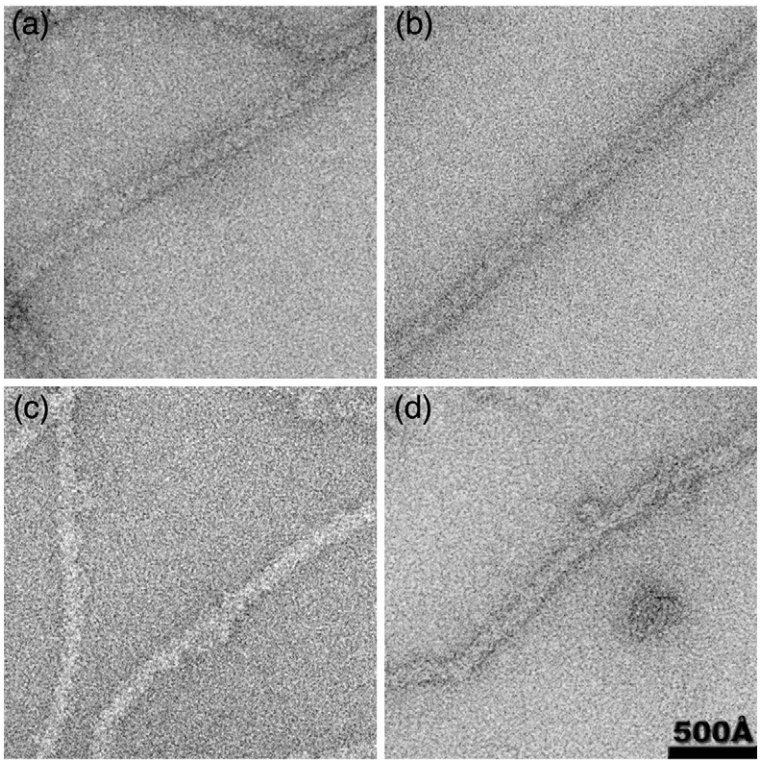


Fig. 1. Electron micrographs of RecA–DNA filaments (a) and RecAΔC17–DNA filaments (b) show strong periodic striations that arise from the one-start right-handed RecA filament helix. These striations disappear when DinI is added to wild-type RecA (c) or RecAΔC17 filaments (d).

large-scale conformational changes to the RecA protomers within the extended RecA filament take place upon the deletion of the 17 terminal residues. The alignment of the RecA protomer from the RecA–dsDNA heteroduplex filament with the crystal structure of *M. smegmatis* RecA[9] places the missing 17 residues in the region spanning from the outer portion of the CTD to the channel in between two adjacent RecA protomers (Fig. 2b, cyan spheres).

Incubation of the RecA or RecAΔC17 filaments with DinI resulted in the disappearance of the helical pattern (Fig. 1c and d), suggesting that DinI was bound to these filaments. We collected 5891 segments of wild-type RecA and 5773 segments of RecAΔC17 filaments decorated with DinI. The 3D reconstructions of the two sets are shown in Fig. 3b and c, respectively. The wild-type RecA–DinI reconstruction (Fig. 3b) showed two regions of density that are absent in the map of pure RecAΔC17 (Fig. 3a): the first site was an attachment to the CTD (Fig. 3b, red arrow), while the second site was a continuous density located in the helical groove (Fig. 3b, blue arrow). A continuous density located in the helical groove was observed in the RecAΔC17–DinI reconstruction (Fig. 3c, blue arrow), although no binding of DinI to RecA's CTD was detected in the overall reconstruction. It was unclear whether the two regions of binding of

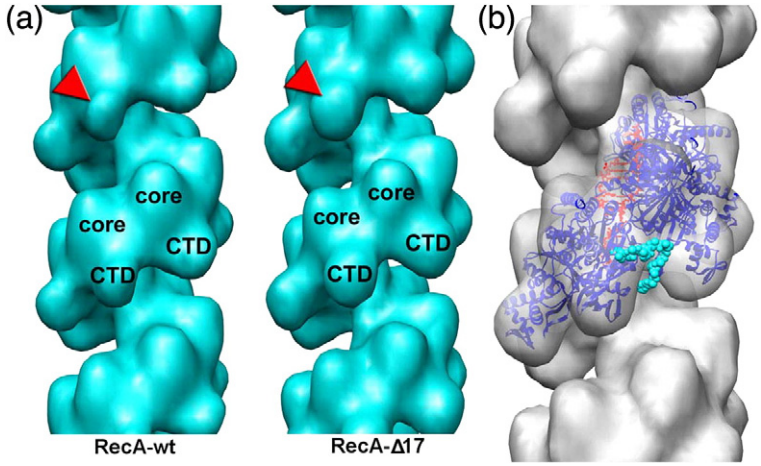


Fig. 2. Three-dimensional reconstructions of RecA and RecAΔC17 filaments (a) are similar in the core region but differ in the CTD region (red arrowheads). The crystal structure of the RecA–dsDNA filament[18] fits without perturbation into the RecAΔC17 reconstruction (b). The RecA protomers are shown as blue ribbons, while the dsDNA molecule is shown in red. The position of the 24 C-terminal residues found ordered in the crystal structures of *M. smegmatis* RecA[9] is shown as cyan spheres.

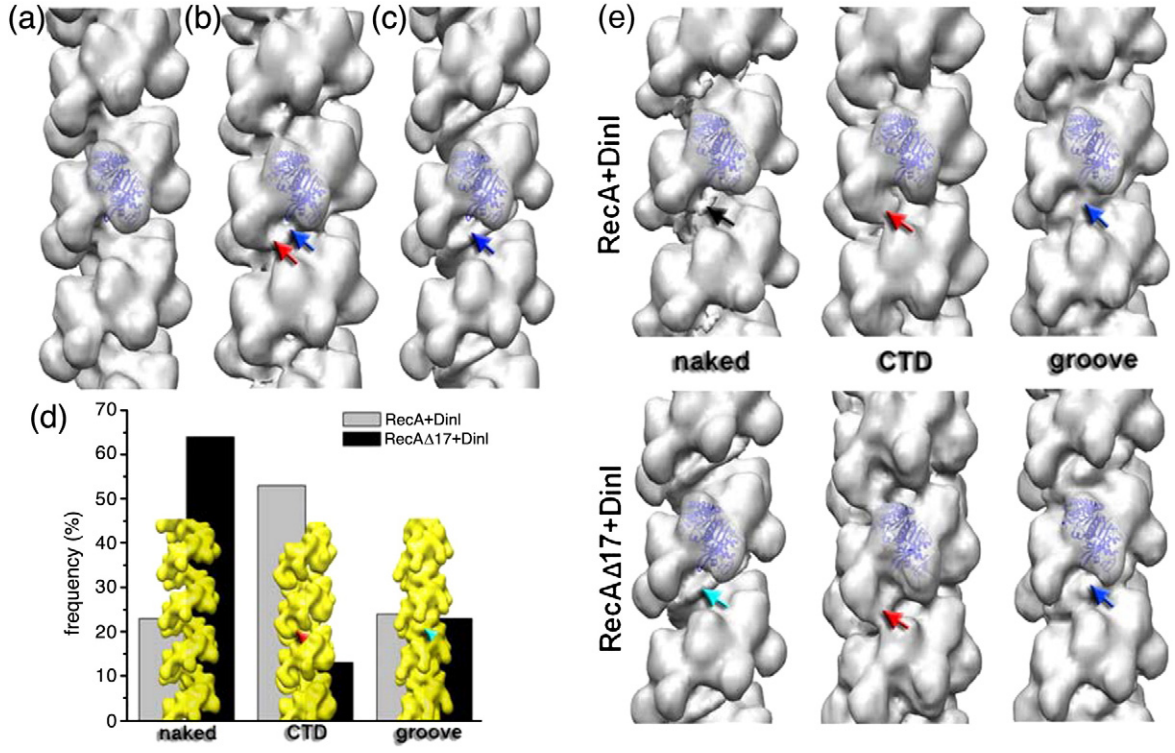


Fig. 3. Comparison of the 3D reconstructions of the pure RecAΔC17 filament (a), RecA–DinI complex (b), and RecAΔC17–DinI complex (c) reveals additional density bound to the CTD of RecA (red arrow), along with the continuous density residing in the helical groove (blue arrows). Cross-correlation sorting using model volumes (d; yellow surfaces) revealed differences in the frequencies of the two modes of DinI binding to RecA (d; gray and black bars). Three-dimensional reconstructions of each of the six classes shown in (d) are shown in (e) as filled surfaces. While the reconstructions of the CTD (red arrows) and the groove (blue arrows) modes from the RecA–DinI and RecAΔC17–DinI complexes are similar, the reconstructions of the naked classes differ. Poorly decorated segments from RecA–DinI filaments have few traces of the DinI bound (black arrow), while such filaments extracted from the RecAΔC17–DinI complex possess continuous density in the helical groove (cyan arrow).

DinI found in the RecA–DinI reconstruction (Fig. 3b, red and blue arrows) reflected a single mode of DinI–RecA interaction or represented a mixture of two distinct modes.

The single-particles approach to helical reconstruction allows us to sort segments of filaments by occupancy and mode of binding. We generated three model volumes (Fig. 3d): a naked RecA filament, a RecA filament having additional density at its CTD (Fig. 3d, red arrowhead), and a RecA filament with a continuous density in the helical groove (Fig. 3d, cyan arrowhead). The three model volumes were projected and cross-correlated with the images of the RecA–DinI and RecAΔC17–DinI complexes. The frequency distribution for such sorting is shown in Fig. 3d as gray and black bars, respectively. The majority of the RecA–DinI images (~54%) had the highest correlation, with the model having additional density attached to the CTD, while a quarter of segments were assigned to the "groove" class (Fig. 3d, gray bars). The deletion of the 17 C-terminal residues did not alter the frequency of the groove mode but significantly reduced the population of the "CTD" class (Fig. 3d, black bars). Each class was iterated in the Iterative Helical Real-Space Reconstruction (IHRSR) procedure starting from a filled featureless cylinder until it had converged to a stable solution. The resultant reconstructions are shown in Fig. 3e. The poorly decorated RecA–DinI filaments yielded a reconstruction possessing weak traces of DinI (Fig. 3e, black arrow), while the same class from the RecAΔC17–DinI complex resulted in a map having continuous additional density in the helical groove (Fig. 3e, cyan arrow). This suggested that the cooperativity of DinI binding to RecA was higher than that to RecAΔC17. The CTD class reconstructions had a substantial additional mass attached to the CTD (Fig. 3e, red arrows). The groove classes from both sets yielded maps having substantial continuous density in the helical groove of the RecA filament (Fig. 3e, blue arrows). Despite similar frequencies of the groove classes (Fig. 3d) and because of substantial additional density in the helical groove of the naked RecAΔC17–DinI class reconstruction, our sorting suggested that the

groove of the RecAΔC17 filaments was more attractive to DinI than that of unmodified RecA filaments.

Since each class was reconstructed from a featureless filled cylinder, the details of the reconstructions reflected the real modes of interaction of DinI with the RecA filament rather than model-biased solutions. We therefore used the reconstructions of the CTD and the groove classes of the RecAΔC17–DinI complex to build atomic models of the two structural modes. The RecA protomer from the crystal structure of the RecA–dsDNA filament[18] was used to model the position of RecA protomers in the RecA–DinI complex while keeping the interface between the adjacent RecA protomers similar to that in the original crystal. Three consecutive RecA protomers docked into the density map are shown in Fig. 4 as magenta, cyan, and orange ribbons. Docking of RecA into the two decorated maps allowed us to determine the density attributed to DinI in each reconstruction. In both modes of binding, the additional density perfectly matched the size and the shape of the DinI molecule (Fig. 4, green ribbons). The models suggested that the two modes were mutually exclusive. That is, a DinI molecule could not be bound to the same RecA protomer in both modes without extensive steric clashes. If DinI were randomly bound to RecA filaments at either of the two sites, we would never be able to sort out the two discrete modes that we observe. Instead, our results are consistent with cooperativity of binding, so that there is predominantly one mode present within the lengths of the segments we are analyzing (~22 RecA subunits). What could be responsible for such cooperativity? In the groove mode (Fig. 4b), there appears to be an interaction between adjacent DinI molecules bound to RecA actin subunits, and such a DinI–DinI interaction could contribute to the cooperative nature of the binding. Since the two DinI molecules do not interact with each other in the CTD mode, it is likely that the cooperativity in interaction in that particular mode must reside mainly within the RecA filament. That is, when DinI binds to one RecA protomer in the CTD mode, structural changes in RecA filament greatly increase the likelihood that DinI will bind to adjacent RecA subunits in this same manner. This is consistent with many articles showing such internal cooperativity within RecA filaments.[33,34]

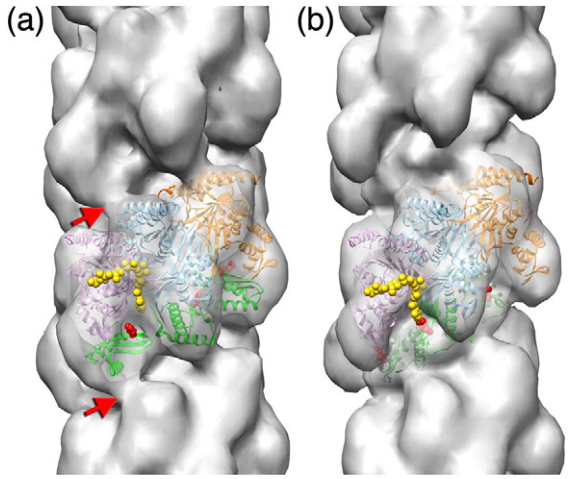


Fig. 4. Three-dimensional reconstructions of the CTD mode (a) and the groove mode (b) are shown with three consecutive RecA protomers docked into the electron density maps (magenta, cyan, and orange ribbons). Three DinI molecules in each mode are shown as green ribbons. The 17 C-terminal residues present in the crystal structure of *M. smegmatis* RecA[9] are shown as yellow spheres. In the CTD mode, the DinI protein bridges adjacent RecA protomers across the helical strand (red arrows). Mutation in R43 (red spheres) significantly diminishes the ability of DinI to stimulate ATP hydrolysis by RecA.

In general, the docking of a high-resolution structure of a protein into a 23-Å-resolution map is quite ambiguous.[35] Due to a substantial asymmetry of the RecA and DinI molecules when filtered to 23 Å, the orientation of both molecules in the resultant atomic models was unambiguous. In addition, the two models are supported by DinI mutagenesis studies, which show that substitution of Arg43 of DinI significantly reduces its ability to stimulate RecA ATPase activity (Supplementary Data). In both atomic models, that residue is located in proximity to the RecA CTD (Fig. 4a and b, red spheres).

We used the recent crystal structure of *M. smegmatis* RecA[9] to reveal the position of the 17 C-terminal residues in our atomic models (Fig. 4, yellow spheres). Interestingly, in both modes, the C-terminus was located far from the DinI molecule (Fig. 4a and b). The removal of the 17 C-terminal residues of RecA did not alter the mode of binding of DinI to RecA; rather, it only changed the frequency of the existing modes (Fig. 3d), suggesting that the C-terminus is not involved in direct interaction with DinI. Why then does the deletion of these C-terminal residues alter the interaction between RecA and DinI? Most of the bacterial RecA proteins contain a high concentration of negatively charged residues at their C-terminus.[10] In all but one RecA crystal structure, this region of RecA has been found to be disordered. The DinI molecule has an extended negatively charged ridge[36] in its C-terminal helix. If the C-terminus of RecA is located in the groove of the filament, electrostatic forces may preclude an extensive binding of DinI in the helical groove and favor the CTD mode of binding. Alternatively, the deletion of the C-terminus may cause conformational changes in RecA, and this could alter the frequency of the two modes. This is consistent with our observations that the deletion of the 17 C-terminal residues stabilizes the CTD of RecA (Fig. 2a). In

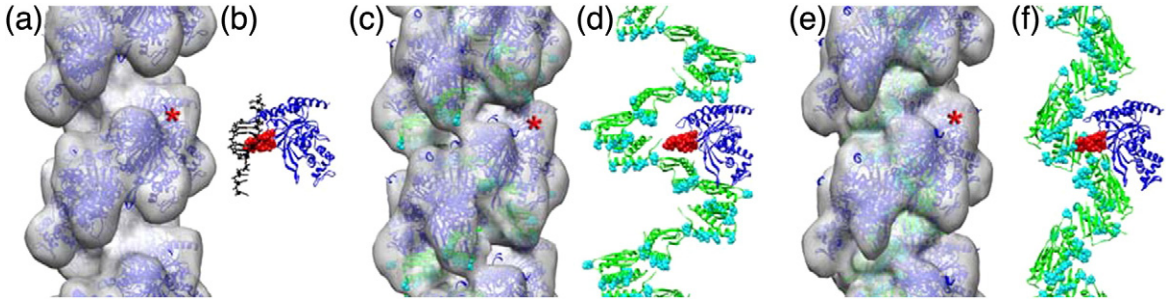


Fig. 5. In the atomic model of the pure RecA filament (a; blue ribbons), the dsDNA molecule (b; black ribbons) is proximal to the L2 loop of RecA (b; red spheres). When DinI binds to RecA in the CTD mode (c and d; green ribbons), the six Asp/Glu residues in the C-terminal helix that form an extended negatively charged ridge[36] (c and d; cyan spheres) are distal from the L2 loop of RecA (d; red spheres). In the atomic model of the groove mode, the negatively charged C-terminal helix forms a continuous helical pattern (e and f; cyan spheres) flanking the L2 region of RecA (f; red spheres). The position of the single RecA protomer (b, d, and f; blue ribbons) is marked with red asterisks in the filament models (a, c, and e).

addition, the extreme C-terminal residues could be making a direct favorable contact with DinI, increasing the frequency of this mode. A high-resolution structure of the RecA–DinI complex is required to distinguish among these possibilities.

It has been shown that DinI, at a low concentration, can stabilize the RecA filament without interfering with LexA cleavage and an ongoing strand exchange reaction.[28] When DinI binds to RecA in the CTD mode, it bridges adjacent RecA protomers across the helical groove (Fig. 4a, red arrows), contributing to intrafilament contacts. Importantly, being bound in this mode leaves the groove available for LexA cleavage[13] and for the invasion of dsDNA into the groove.

An extensive interaction between the adjacent DinI molecules in the groove mode may increase the affinity of DinI for the RecA filament. Because of the preferential binding of DinI to RecAΔC17 in the groove mode, one would expect the RecAΔC17–DinI complex to be more stable than the RecA–DinI complex. Strikingly, the RecAΔC17–DinI complex was shown to be 100 times more stable than the one formed with unmodified RecA.[28]

When DNA in the atomic model of the RecAΔC17 filament is positioned as in the crystal structure,[18] it is proximal to the L2 loop region of RecA (Fig. 5b, red spheres), which has been implicated in DNA binding[37,38] and homologous pairing.[39] The solution structure of DinI shows that six Asp/Glu residues in the C-terminal helix form an extended negatively charged ridge[36] (Fig. 5c–f, cyan spheres), and this ridge was proposed to compete with ssDNA for binding to the RecA L2 region.[27] In the CTD mode, the negatively charged region of DinI is located at the outer surface of the RecA filament (Fig. 5d, cyan spheres) and is far from the L2 loop of RecA (Fig. 5d, red spheres). In the groove mode, the negatively charged C-terminal helix forms a continuous helical path (Fig. 5f, cyan spheres) flanking the L2 region of RecA (Fig. 5f, red spheres). Our data show that when DinI is bound to the RecA filament in the groove mode, it can compete with the DNA for binding to the L2 loop. This interaction may facilitate the dissociation of RecA subunits from the nucleoprotein filament.

RecX protein is a suppressor of the SOS response and inhibits LexA cleavage and strand exchange reaction by depolymerization of RecA filaments.[21,23] When the RecA filament is stabilized with AMP-PNP, RecX produces a continuous density that forms a block across the deep helical groove of the RecA filament.[13] Such a mode of binding intuitively explains how RecX can inhibit LexA cleavage by simply blocking the penetration of LexA into the groove of the filament. It has been suggested recently that the positively charged concave surface of RecX can make an extensive contact with the DNA phosphate backbone.[40] DinI binds to RecAΔC17 filaments presumably in the groove mode, and its position on the RecA filament in that mode (Fig. 4b) is very similar to that found for RecX protein.[13]

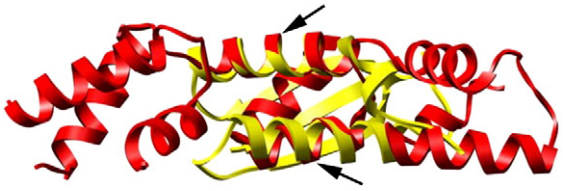


Fig. 6. The RecX protein (red) consists of three domains, where each domain contains three α-helices.[40] The structural similarity of each of the three domains has suggested gene triplication. The DinI protein (yellow) is a single domain containing two α-helices and a single β-sheet.[36] Two of the three RecX helices superimpose quite well on the two helices in DinI, raising the possibility of homology for this RecA binding domain. Bottom: DinI helix containing residues 17–31 is superimposed on the RecX helix containing residues 81–90. Top: The DinI helix containing residues 57–73 is superimposed on the RecX helix containing residues 63–76.

Consistent with this picture, DinI inhibits the ability of RecAΔC17 to catalyze the strand exchange reaction.[28] RecX contains three small domains, each containing three helices. The protein appears to have been the result of gene triplication, as the three domains show strong structural homology. The two helices in DinI align extremely well with two of the three helices in each of the RecX domains, and the fit of DinI to the central domain of RecX is shown (Fig. 6). Whether this represents a convergent evolution or a distant homology cannot be determined at this time.

Our data show that the C-terminus of RecA is involved in modulating the RecA–DinI interaction. In the groove mode, DinI resides deeply in the groove of the RecA filament, with its negatively charged C-terminal helix proximal to the L2 loop of RecA. This supports the original suggestion that the negatively charged C-terminal helix of DinI mimics DNA and interferes with the activation of RecA.[27] We suggest that the negatively charged C-terminus of RecA prevents DinI from entering the groove and protects the RecA filament from depolymerization, since the deletion of the 17 C-terminal residues of RecA favors the groove mode of binding. How can such a regulatory mechanism work in the cell lacking truncated RecA protein? The deletion of the 17 C-terminal residues in RecA *in vitro* may mimic conformational changes in the RecA filament that otherwise are triggered by regulatory proteins such as RecO and RecR. The enhanced binding of DinI to RecA at the late stages of the SOS response[27] strongly argues for the existence of one or more modulators of the DinI–RecA interaction, since DinI synthesis starts at the early stages of the SOS response.

Materials and Methods

Cloning

To clone an *E. coli dinI* gene that encodes the R43A mutant protein, we used the wild-type *dinI* gene in pEAW334 as template in a PCR, with the upstream primer consisting of the *dinI* gene starting at the BsaAI restriction enzyme site at base 115 and including at least 10 bases after the changed bases. For R43A, the CGT starting at base 126 of the *dinI* gene was changed to GCT. The downstream primer consisted of an EcoRI restriction enzyme site and the last 19 bases of the *dinI* gene. The PCR product was digested with BsaAI and EcoRI and ligated to pEAW340 cut with the same restriction enzymes. The plasmid designated pEAW340 is the wild-type *dinI* gene inserted into pUC19 sites. The presence of *dinI* mutation was confirmed by a direct sequencing of the resulting plasmids. The mutant *dinI* gene was then subcloned into pET21A cut at the NdeI and EcoRI sites, and the *dinI* genes of the resulting plasmids were again directly sequenced. The plasmid with *dinI* R43A was designated pEAW533.

To create His-tagged versions of the mutant and wild-type DinI proteins, we used primers (5′ CCTAAGCCATATGCGAATTGAAGTCACC-3′ and 5′ GGATATCCTCGAGTTCGCTGACAACCAGTC-3′) to amplify mutant *dinI* genes from their respective plasmids (pEAWs 533 and 334) and to append flanking NdeI and XhoI restriction sites. PCR products and pET-21b(+) (Novagen) were cut with NdeI and XhoI and ligated. The resulting plasmids were sequenced to ensure the integrity of the *dinI* coding region. The above cloning procedure resulted in mutant *dinI* genes with six His codons at the 3′ end of the *dinI* coding sequence, followed by a stop codon.

DNA substrates

Poly-dT DNA was purchased from Amersham Biosciences. Its average length was 319 nucleotides. The concentration of poly-dT was reported in terms of micromolar nucleotides.

Proteins

Untagged wild-type DinI protein was overexpressed in *E. coli* STL2669/pT7pol26 cells. Ten liters of culture was grown in LB to an OD_{600} of 0.5, and DinI protein expression was induced with 0.4 mM isopropyl-1-thio-β-D-galactopyranoside. Approximately 15–20 g of cells was harvested by centrifugation following 3 h of incubation at 37 °C. Cells were flash-frozen in liquid N_2 and stored at −80 °C. Cells were thawed overnight on ice in a buffer containing 250 mM Tris–Cl (80% cation, pH 7.8) and 25% wt/vol sucrose. The cells were resuspended to 20% wt/vol and lysed via sonication with a Fisher Scientific Sonic Dismembrator Model 500 at 60% output (five times) for 1-min segments with alternating 0.5-s on/off pulses. Lysed cells were centrifuged for 60 min at 16,000 rpm in a Beckman JLA-16.25 rotor at 4 °C. The lysis supernatant was dialyzed against P-buffer [10 mM KH_2PO_4, 10 mM K_2HPO_4, 0.1 mM ethylenediaminetetraacetic acid, 10% wt/vol glycerol, and 1 mM dithiothreitol (DTT)] and run over a ceramic hydroxyapatite column. Wild-type DinI protein was not retained by the hydroxyapatite, and the wash fractions containing DinI were dialyzed against R-buffer [20 mM Tris–Cl 80% cation (pH 7.8), 0.1 mM ethylenediaminetetraacetic acid, 10% wt/vol glycerol, and 1 mM DTT]. DinI was then applied to a Q-Sepharose anion-exchange column and eluted with a linear gradient from R-buffer to R-buffer + 1 M KCl. Gradient fractions containing DinI protein were dialyzed back into R-buffer and run over a heparin Sepharose column. Heparin Sepharose flow-through fractions containing DinI protein were concentrated on a 1-ml Q-Sepharose column with a step gradient from R-buffer to R-buffer + 1 M KCl. The concentrated DinI was run over a Hi-Prep Sephacryl 16/60 S-100 size-exclusion column in R-buffer + 200 mM KCl. Fractions containing pure wild-type DinI protein were pooled and dialyzed into R-buffer for storage. The wild-type DinI protein was free of detectable ssDNA nuclease activity.

To overexpress the His-tagged DinI proteins, we transformed plasmids bearing the *dinI* genes into the *E. coli* STL327(DE3) strain, which was grown, harvested, and frozen as described above for untagged wild-type DinI.

Five milliliters of lysis buffer [50 mM potassium phosphate, 300 mM NaCl, 10 mM imidazole, and 10% wt/vol glycerol (pH 8.0)] was added per gram of cell pellets to resuspend the pellets. Cells were thawed overnight on ice, with gentle stirring. The protease inhibitors E-64 and leupeptin (0.5 μg ml^{-1}), and pepstatin (1 μM) were added to fully resuspended cells. The cells were lysed at 4 °C for 2 h with lysozyme at a final concentration of 4 mg ml^{-1}. The cells were sonicated and centrifuged as described above. The supernatant was incubated in batches with ~5 ml of Ni-NTA slurry preequilibrated with lysis buffer for 1 h at 4 °C. The slurry was poured into a solid support, then washed with 30 column volumes of wash buffer [50 mM potassium phosphate, 0.3 M NaCl, 20 mM imidazole, and 10% wt/vol glycerol (pH 8.0)]. Histidine-tagged DinI protein was eluted with 5 column volumes of elution buffer (same as wash buffer, except with 500 mM imidazole). Wild-type histidine-tagged DinI (wild-type His–DinI) was dialyzed against R-buffer and eluted from a 1-ml Q-Sepharose column with a linear gradient from R-buffer to R-buffer + 1 M KCl. Fractions containing wild-type His–DinI were run over a Hi-Prep Sephacryl 16/60 S-100 size-exclusion column and a ceramic hydroxyapatite column, and concentrated on a 1-ml Q-Sepharose column with a step gradient, as described above. Eluted wild-type His–DinI protein was dialyzed against R-buffer for storage. His–R43A DinI protein was purified as for the wild-type His-tagged protein, except that it was not concentrated on the 1-ml Q-Sepharose after the ceramic hydroxyapatite column. All purified proteins were flash-frozen with liquid N_2 and stored at −80 °C. Each was determined by SDS-PAGE to be pure and had no detectable ssDNA nuclease activity at 20 μM DinI after 2 h of incubation at 37 °C. The theoretical extinction coefficient of 1.44×10^4 M^{-1} cm^{-1} at 280 nm for wild-type DinI calculated using the ProtParam tool (from the ExPASy Web site) was used to determine the concentration of all DinI proteins.

Each DinI protein was diluted in R-buffer to a concentration between 0.1 and 0.2 mg ml^{-1} and was submitted to the Biophysics Instrumentation Facility at University of Wisconsin-Madison to check for proper folding by circular dichroism (CD). All data were collected in 0.1-cm cuvettes at 37 °C, with a 1-nm bandpass at 1-nm intervals and a 5-s averaging time at each point. An R-buffer blank was recorded and subtracted from each spectrum. Conversion into molar ellipticity was carried out using DinI concentrations measured as described above and a mean residue weight of 110 Da. The CD spectra for the DinI proteins were normalized by arbitrarily setting the molar ellipticity at 218 nm to −1 deg cm^2 $dmol^{-1}$.

ATP hydrolysis assays to monitor the effect of the DinI mutant proteins on RecA

A spectrophotometric coupled enzyme assay was used to measure RecA-catalyzed ATP hydrolysis.[41,42] The ADP produced by hydrolysis was converted back into ATP by the enzyme pyruvate kinase and by the substrate phosphoenolpyruvate. The resultant pyruvate was reduced to lactate by lactate dehydrogenase using NADH as reducing agent. The conversion of NADH into NAD^+ was monitored as a decrease in absorbance at 380 nm on a Varian Cary 300 instrument equipped with a temperature controller and a 12-position cell changer. The cell pathlength was 0.5 cm. The concentration of oxidized NADH and thus the concentration of hydrolyzed ATP were calculated from the NADH extinction coefficient $\varepsilon_{380} = 1.21$ mM^{-1} cm^{-1}.

Each ATP hydrolysis assay contained a reaction mixture of 25 mM Tris·OAc (88% cation, pH 7.5), 10 mM magnesium acetate, 4 mM potassium glutamate, 5% (wt/vol) glycerol, 1 mM DTT, 3.5 mM phosphoenolpyruvate, 10 U ml^{-1} pyruvate kinase, 10 U ml^{-1} lactate dehydrogenase, 1.5 mM NADH, 3 μM poly-dT, and 3 mM ATP. DinI proteins or compensating storage buffer was incubated with the above reaction mixture at 37 °C for 10 min. The DinI concentration was varied from 0 to 20 μM. Wild-type RecA protein was then added to a final concentration of 1 μM. RecA-catalyzed ATP hydrolysis was monitored at 37 °C until NADH had been exhausted. The k_{cat} for RecA-catalyzed ATP hydrolysis at various DinI concentrations was calculated from the rate of ATP hydrolysis divided by the concentration of RecA binding sites on poly-dT.

Electron microscopy and image analysis

The RecA–dsDNA–AMPPNP and RecAΔC17–dsDNA–AMPPNP complexes were incubated in 25 mM triethanolamine–HCl (Fisher Scientific) buffer (pH 7.2) at 37 °C for 10 min, with [RecA] or [RecAΔC17] of 2 μm, RecA/calf thymus dsDNA (Sigma) ratio of 40:1 (wt/wt), 1.5 mM AMP-PNP (Sigma), and 2.5 mM magnesium acetate (Sigma). The DinI complexes were formed in the same manner, except that 20 μM DinI was present. Samples were applied to carbon-coated grids and stained with 2% (wt/vol) uranyl acetate (wt/vol). Images were recorded on film using a Tecnai 12 electron microscope operating at 80 keV at a nominal magnification of 30,000×. Negatives were scanned with a Nikon Coolscan 8000 densitometer at a raster of 4.2 Å/pixel. SPIDER[43] was used for image processing. Segments of the filaments (80 × 80 pixels) of RecA ($n = 5300$) or RecAΔ17 ($n = 5301$) formed on dsDNA in the presence of AMP-PNP were extracted from the micrographs and reconstructed using the IHRSR method.[44] Both sets converged to the same helical parameters and yielded a twist of 58.5° and an axial rise of 15 Å. Segments (80 × 80 pixels) of RecA–dsDNA–AMP-PNP ($n = 5891$) or RecAΔ17–dsDNA–AMP-PNP ($n = 5773$) decorated with DinI protein were extracted from micrographs, and overall reconstructions were calculated (Fig. 3b and c, respectively). Both sets converged to the same helical symmetry of 59°/15 Å with the IHRSR method. The central protomer from the RecA–dsDNA crystal structure (PDB ID: 3CMU) was used to generate a model RecA filament. The DinI solution structure (PDB ID: 1GHH) was used to build up two models—with the DinI attached to the CTD (Fig. 3d, red arrowhead) or located deeply in the groove of the RecA filament (Fig. 3d, cyan arrowhead). The model of the RecA filament, along with the two decorated models, was used as reference in cross-correlation sorting. The three reference volumes were scaled to 4.2 Å/pixel and projected onto 80 × 80 pixel images with an azimuthal rotational increment of 4°, generating 270 reference projections (3 × 90 pixels). RecA–dsDNA–AMP-PNP–DinI and RecAΔ17–dsDNA–AMP-PNP–DinI segments were cross-correlated with the 270

reference projections. Reconstructions were independently generated for each class (Fig. 3e) starting from a featureless filled cylinder. The two naked classes ($n=1375$ and $n=3683$, respectively) both converged to a symmetry of 59°/15 Å. The two CTD classes ($n=3094$ and $n=766$, respectively) yielded symmetries of 58.7°/14.7 Å and 58.4°/14.4 Å, while the groove classes ($n=1422$ and $n=1324$, respectively) converged to helical parameters of 58.8°/14.6 Å and 58.5°/14.8 Å. The resolution of the reconstructions was judged to be ~23 Å using the criterion FSC = 0.5.

UCSF Chimera software[45] was used to fit the high-resolution structures of RecA and DinI into the experimental density maps. Atomic coordinates from crystal structures were converted into density maps, and these were filtered to the resolution of the experimental map and docked manually.

Supplementary materials related to this article can be found online at doi:10.1016/j.jmb.2011.03.046

References

1. Kowalczykowski, S. C. & Eggleston, A. K. (1994). Homologous pairing and DNA strand-exchange proteins. *Annu. Rev. Biochem.* **63**, 991–1043.
2. Little, J. W. & Mount, D. W. (1982). The SOS regulatory system of *Escherichia coli*. *Cell*, **29**, 11–22.
3. Smith, K. C. & Wang, T. C. (1989). recA-dependent DNA repair processes. *BioEssays*, **10**, 12–16.
4. Story, R. M. & Steitz, T. A. (1992). Structure of the recA protein–ADP complex. *Nature*, **355**, 374–376.
5. Datta, S., Prabu, M. M., Vaze, M. B., Ganesh, N., Chandra, N. R., Muniyappa, K. & Vijayan, M. (2000). Crystal structures of *Mycobacterium tuberculosis* RecA and its complex with ADP–AlF(4): implications for decreased ATPase activity and molecular aggregation. *Nucleic Acids Res.* **28**, 4964–4973.
6. Xing, X. & Bell, C. E. (2004). Crystal structures of *Escherichia coli* RecA in complex with MgADP and MnAMP-PNP. *Biochemistry*, **43**, 16142–16152.
7. Xing, X. & Bell, C. E. (2004). Crystal structures of *Escherichia coli* RecA in a compressed helical filament. *J. Mol. Biol.* **342**, 1471–1485.
8. Datta, S., Krishna, R., Ganesh, N., Chandra, N. R., Muniyappa, K. & Vijayan, M. (2003). Crystal structures of *Mycobacterium smegmatis* RecA and its nucleotide complexes. *J. Bacteriol.* **185**, 4280–4284.
9. Krishna, R., Manjunath, G. P., Kumar, P., Surolia, A., Chandra, N. R., Muniyappa, K. & Vijayan, M. (2006). Crystallographic identification of an ordered C-terminal domain and a second nucleotide-binding site in RecA: new insights into allostery. *Nucleic Acids Res.* **34**, 2186–2195.
10. Roca, A. I. & Cox, M. M. (1997). RecA protein: structure, function, and role in recombinational DNA repair. *Prog. Nucleic Acid Res. Mol. Biol.* **56**, 129–223.
11. Fernandez de Henestrosa, A. R., Ogi, T., Aoyagi, S., Chafin, D., Hayes, J. J., Ohmori, H. & Woodgate, R. (2000). Identification of additional genes belonging to the LexA regulon in *Escherichia coli*. *Mol. Microbiol.* **35**, 1560–1572.
12. Little, J. W. (1984). Autodigestion of lexA and phage repressors. *Proc. Natl Acad. Sci. USA*, **81**, 1375–1379.
13. VanLoock, M. S., Yu, X., Yang, S., Galkin, V. E., Huang, H., Rajan, S. S. *et al.* (2003). Complexes of RecA with LexA and RecX differentiate between active and inactive RecA nucleoprotein filaments. *J. Mol. Biol.* **333**, 345–354.
14. Kowalczykowski, S. C., Clow, J. & Krupp, R. A. (1987). Properties of the duplex DNA-dependent ATPase activity of *Escherichia coli* RecA protein and its role in branch migration. *Proc. Natl Acad. Sci. USA*, **84**, 3127–3131.
15. Lusetti, S. L., Shaw, J. J. & Cox, M. M. (2003). Magnesium ion-dependent activation of the RecA protein involves the C terminus. *J. Biol. Chem.* **278**, 16381–16388.
16. Tateishi, S., Horii, T., Ogawa, T. & Ogawa, H. (1992). C-terminal truncated *Escherichia coli* RecA protein RecA5327 has enhanced binding affinities to single- and double-stranded DNAs. *J. Mol. Biol.* **223**, 115–129.
17. Eggler, A. L., Lusetti, S. L. & Cox, M. M. (2003). The C terminus of the *Escherichia coli* RecA protein modulates the DNA binding competition with single-stranded DNA-binding protein. *J. Biol. Chem.* **278**, 16389–16396.
18. Chen, Z., Yang, H. & Pavletich, N. P. (2008). Mechanism of homologous recombination from the RecA–ssDNA/dsDNA structures. *Nature*, **453**, 489–494.
19. Sano, Y. (1993). Role of the recA-related gene adjacent to the recA gene in *Pseudomonas aeruginosa*. *J. Bacteriol.* **175**, 2451–2454.
20. Vierling, S., Weber, T., Wohlleben, W. & Muth, G. (2000). Transcriptional and mutational analyses of the *Streptomyces lividans* recX gene and its interference with RecA activity. *J. Bacteriol.* **182**, 4005–4011.
21. Stohl, E. A., Brockman, J. P., Burkle, K. L., Morimatsu, K., Kowalczykowski, S. C. & Seifert, H. S. (2003). *Escherichia coli* RecX inhibits RecA recombinase and coprotease activities *in vitro* and *in vivo*. *J. Biol. Chem.* **278**, 2278–2285.
22. Drees, J. C., Lusetti, S. L., Chitteni-Pattu, S., Inman, R. B. & Cox, M. M. (2004). A RecA filament capping mechanism for RecX protein. *Mol. Cell*, **15**, 789–798.
23. Drees, J. C., Lusetti, S. L. & Cox, M. M. (2004). Inhibition of RecA protein by the *Escherichia coli* RecX protein: modulation by the RecA C terminus and filament functional state. *J. Biol. Chem.* **279**, 52991–52997.
24. Lewis, L. K., Harlow, G. R., Gregg-Jolly, L. A. & Mount, D. W. (1994). Identification of high affinity binding sites for LexA which define new DNA damage-inducible genes in *Escherichia coli*. *J. Mol. Biol.* **241**, 507–523.
25. Yasuda, T., Nagata, T. & Ohmori, H. (1996). Multicopy suppressors of the cold-sensitive phenotype of the pcsA68 (dinD68) mutation in *Escherichia coli*. *J. Bacteriol.* **178**, 3854–3859.
26. Yasuda, T., Morimatsu, K., Kato, R., Usukura, J., Takahashi, M. & Ohmori, H. (2001). Physical interactions between DinI and RecA nucleoprotein filament for the regulation of SOS mutagenesis. *EMBO J.* **20**, 1192–1202.
27. Voloshin, O. N., Ramirez, B. E., Bax, A. & Camerini-Otero, R. D. (2001). A model for the abrogation of the SOS response by an SOS protein: a negatively charged

helix in DinI mimics DNA in its interaction with RecA. *Genes Dev.* **15**, 415–427.
28. Lusetti, S. L., Voloshin, O. N., Inman, R. B., Camerini-Otero, R. D. & Cox, M. M. (2004). The DinI protein stabilizes RecA protein filaments. *J. Biol. Chem.* **279**, 30037–30046.
29. Craig, N. L. & Roberts, J. W. (1981). Function of nucleotide triphosphate and polynucleotide in *E. coli* RecA protein-directed cleavage of phage lambda repressor. *J. Biol. Chem.* **256**, 8039–8044.
30. Campbell, M. J. & Davis, R. W. (1999). On the *in vivo* function of the RecA ATPase. *J. Mol. Biol.* **286**, 437–445.
31. VanLoock, M. S., Yu, X., Yang, S., Lai, A. L., Low, C., Campbell, M. J. & Egelman, E. H. (2003). ATP-mediated conformational changes in the RecA filament. *Structure (Cambridge)*, **11**, 187–196.
32. Yu, X. & Egelman, E. H. (1991). Removal of the RecA C-terminus results in a conformational change in the RecA–DNA filament. *J. Struct. Biol.* **106**, 243–254.
33. Weinstock, G. M., McEntee, K. & Lehman, I. R. (1981). Hydrolysis of nucleoside triphosphates catalyzed by the recA protein of *Escherichia coli*. Steady state kinetic analysis of ATP hydrolysis. *J. Biol. Chem.* **256**, 8845–8849.
34. De Zutter, J. K. & Knight, K. L. (1999). The hRad51 and RecA proteins show significant differences in cooperative binding to single-stranded DNA. *J. Mol. Biol.* **293**, 769–780.
35. Egelman, E. H. (2008). Problems in fitting high resolution structures into electron microscopic reconstructions. *HFSP J.* **2**, 324–331.
36. Ramirez, B. E., Voloshin, O. N., Camerini-Otero, R. D. & Bax, A. (2000). Solution structure of DinI provides insight into its mode of RecA inactivation. *Protein Sci.* **9**, 2161–2169.
37. Wang, Y. & Adzuma, K. (1996). Differential proximity probing of two DNA binding sites in the *Escherichia coli* recA protein using photo-cross-linking methods. *Biochemistry*, **35**, 3563–3571.
38. Malkov, V. A. & Camerini-Otero, R. D. (1995). Photocross-links between single-stranded DNA and *Escherichia coli* RecA protein map to loops L1 (amino acid residues 157–164) and L2 (amino acid residues 195–209). *J. Biol. Chem.* **270**, 30230–30233.
39. Wang, L., Voloshin, O. N., Stasiak, A. & Camerini-Otero, R. D. (1998). Homologous DNA pairing domain peptides of RecA protein: intrinsic propensity to form beta-structures and filaments. *J. Mol. Biol.* **277**, 1–11.
40. Ragone, S., Maman, J. D., Furnham, N. & Pellegrini, L. (2008). Structural basis for inhibition of homologous recombination by the RecX protein. *EMBO J.* **27**, 2259–2269.
41. Lindsley, J. E. & Cox, M. M. (1990). Assembly and disassembly of RecA protein filaments occur at opposite filament ends. Relationship to DNA strand exchange. *J. Biol. Chem.* **265**, 9043–9054.
42. Morrical, S. W., Lee, J. & Cox, M. M. (1986). Continuous association of *Escherichia coli* single-stranded DNA binding protein with stable complexes of recA protein and single-stranded DNA. *Biochemistry*, **25**, 1482–1494.
43. Frank, J., Radermacher, M., Penczek, P., Zhu, J., Li, Y., Ladjadj, M. & Leith, A. (1996). SPIDER and WEB: processing and visualization of images in 3D electron microscopy and related fields. *J. Struct. Biol.* **116**, 190–199.
44. Egelman, E. H. (2000). A robust algorithm for the reconstruction of helical filaments using single-particle methods. *Ultramicroscopy*, **85**, 225–234.
45. Pettersen, E. F., Goddard, T. D., Huang, C. C., Couch, G. S., Greenblatt, D. M., Meng, E. C. & Ferrin, T. E. (2004). UCSF Chimera—a visualization system for exploratory research and analysis. *J. Comput. Chem.* **25**, 1605–1612.